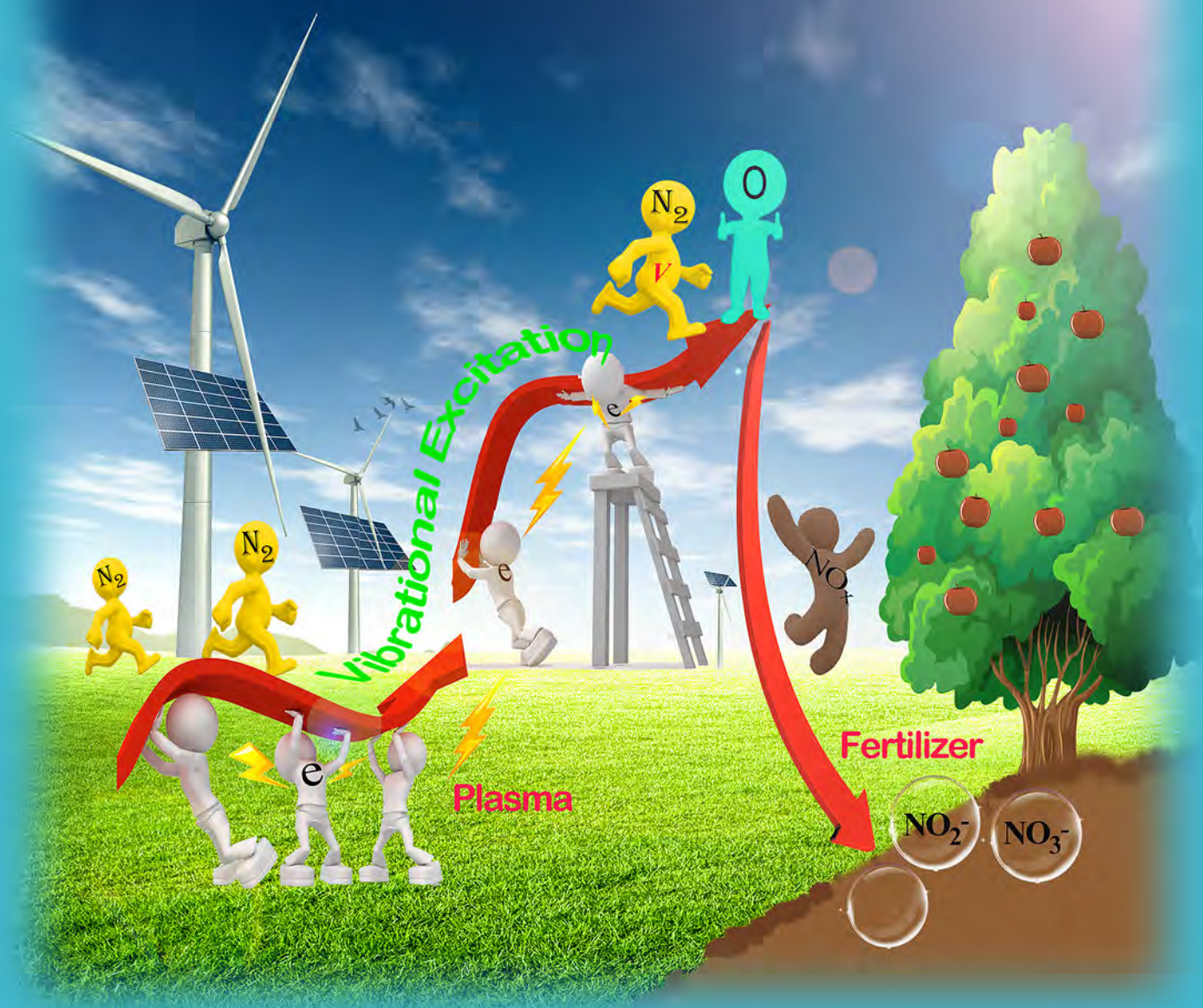


CHEMISTRY & SUSTAINABILITY

# CHEMSUSCHEM

ENERGY & MATERIALS



10/2017

Front Cover Picture:

*Wang et al.*

Nitrogen Fixation by Gliding Arc Plasma:  
Better Insight by Chemical Kinetics Modelling

WILEY-VCH

[www.chemsuschem.org](http://www.chemsuschem.org)

A Journal of



# Nitrogen Fixation by Gliding Arc Plasma: Better Insight by Chemical Kinetics Modelling



Dr. Weizong Wang



Bhaskar Patil



Stijn Heijkers



Prof. Dr. Volker Hessel

Prof. Dr. Annemie  
Bogaerts

Invited for this month's cover is the group of Prof. Dr. Annemie Bogaerts at the University of Antwerp and their collaborators at Eindhoven University of Technology in the laboratory of Prof. Dr. Volker Hessel. The cover image shows that gliding arc plasma leads to energy efficient nitrogen fixation by promoting the vibrational excitation of  $N_2$ . The Full Paper itself is available at [10.1002/cssc.201700095](https://doi.org/10.1002/cssc.201700095).

## What prompted you to investigate this topic/problem?

Considering the increasing demand of fertilizers as well as the high-energy intensity and environmental concerns triggered by industrial nitrogen fixation (i.e., the Haber–Bosch process), there is an urgent need to develop and integrate more sustainable processes of nitrogen fixation. Gliding arc plasma-based nitric oxide synthesis offers unique perspectives for this purpose, but the underlying mechanisms are clearly not yet understood. Hence, we wanted to elucidate the plasma chemistry by a combination of experiments and computations, to provide the necessary insights for gliding arc plasma-based nitrogen fixation. Our work also allows us to propose possible solutions on how to further improve the performance of gliding arc plasma technology.

## What is the most significant result of this study?

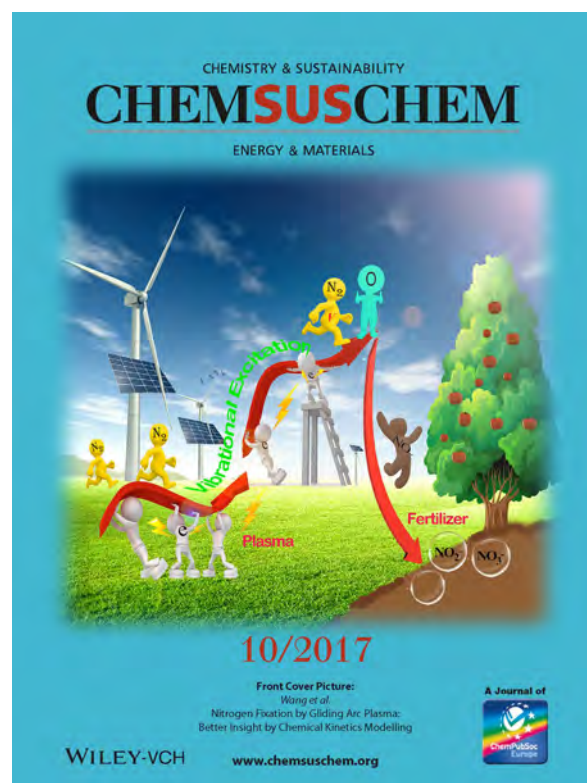
Our results clearly reveal that vibrational excitation of  $N_2$  can help to overcome the reaction energy barrier of the non-thermal Zeldovich mechanism  $O + N_2(V) \rightarrow NO + N$  and can thus significantly enhance the nitric oxide synthesis in the gliding arc plasma. This provides an energy efficient pathway for nitrogen fixation using air as raw material.

## What future opportunities do you see (in the light of the results presented in this paper)?

If electricity from sustainable energy sources (wind and solar) is used, the intrinsic potential of gliding arc plasma-based nitrogen fixation can provide a promising opportunity for producing nitrogenous fertilizer in remote locations by just using small-scale plants, which offer farmers a new source of revenue from their land. This helps to come up with realistic scenarios of entering a cutting-edge innovation in new business cases of plasma agriculture, in which low-temperature plasma technology might play an important role.

## Acknowledgements

The authors appreciate financial supports by the European Marie Skłodowska-Curie Individual Fellowship “GlidArc” within Horizon 2020 (Grant No.657304), the FWO project (Grant G.0383.16N) and the EU project MAPSYN: Microwave, Acoustic, and Plasma assisted SYNthesis (Grant No.CP-IP 309376) under the 7th Framework Programme. The calculations were performed using the Turing HPC infrastructure at the CalcUA core facility of the Universiteit Antwerpen (UAntwerpen), a division of the Flemish Supercomputer Center VSC, funded by the Hercules Foundation, the Flemish Government (department EW1) and the UAntwerpen.





VIP Very Important Paper



# Nitrogen Fixation by Gliding Arc Plasma: Better Insight by Chemical Kinetics Modelling

Weizong Wang,<sup>\*[a]</sup> Bhaskar Patil,<sup>[b]</sup> Stjin Heijkers,<sup>[a]</sup> Volker Hessel,<sup>[b]</sup> and Annemie Bogaerts<sup>\*[a]</sup>

The conversion of atmospheric nitrogen into valuable compounds, that is, so-called nitrogen fixation, is gaining increased interest, owing to the essential role in the nitrogen cycle of the biosphere. Plasma technology, and more specifically gliding arc plasma, has great potential in this area, but little is known about the underlying mechanisms. Therefore, we developed a detailed chemical kinetics model for a pulsed-power gliding-arc reactor operating at atmospheric pressure for nitrogen oxide synthesis. Experiments are performed to validate the model and reasonable agreement is reached between the calculated and measured NO and NO<sub>2</sub> yields and the corresponding energy efficiency for NO<sub>x</sub> formation for different N<sub>2</sub>/O<sub>2</sub> ratios, indicating that the model can provide a realistic picture of the plasma chemistry. Therefore, we can use the model to

investigate the reaction pathways for the formation and loss of NO<sub>x</sub>. The results indicate that vibrational excitation of N<sub>2</sub> in the gliding arc contributes significantly to activating the N<sub>2</sub> molecules, and leads to an energy efficient way of NO<sub>x</sub> production, compared to the thermal process. Based on the underlying chemistry, the model allows us to propose solutions on how to further improve the NO<sub>x</sub> formation by gliding arc technology. Although the energy efficiency of the gliding-arc-based nitrogen fixation process at the present stage is not comparable to the world-scale Haber–Bosch process, we believe our study helps us to come up with more realistic scenarios of entering a cutting-edge innovation in new business cases for the decentralised production of fertilisers for agriculture, in which low-temperature plasma technology might play an important role.

## Introduction

Nitrogen is an essential component for all forms of life because it is required to biosynthesise basic building blocks of plants and living organisms. The latter can consume nitrogen in a usable form, obtained by chemical reaction with oxygen or hydrogen or carbon. Therefore, we find nitrogen compounds in plant cells, amino acids, proteins and nucleic acids. In the earth's atmosphere, there is an abundant supply of nitrogen—78.08% of air is composed of molecular nitrogen (N<sub>2</sub>). However, this most abundant nitrogen source is not available to the majority of living organisms because it is extremely difficult to break its triple bond and very stable electronic configuration, which makes almost any first reaction step of the conversion very energy demanding. As a result, nitrogen fixation (NF), which converts nitrogen molecules into simple nitrogen compounds, such as ammonia or nitric oxide that can be further

used as precursors for the synthesis or biosynthesis of more complex molecules, is very significant. However, it is the most challenging step of nitrogen utilization by living organisms.<sup>[1]</sup>

The conventional Haber–Bosch (H–B) process of the binding of nitrogen with hydrogen to produce ammonia at high pressure and temperature is the most significant process to produce fertilisers.<sup>[2]</sup> It is expected that the global ammonia capacity will increase from 204.2 million tons per year in 2013 to 249.4 million tons by 2018.<sup>[3]</sup> Hence, the amount of synthetic nitrogen obtained by human activities has exceeded natural biological fixation.<sup>[4]</sup> From an energy point of view, industrial ammonia synthesis is the most energy intensive chemical process. The H–B process consumes 1–2% of the world's total energy production and utilises 2–3% of the total natural gas output. Furthermore, it emits more than 300 million metric tons of carbon dioxide.<sup>[5,6]</sup>

Considering the increasing demand of fertilisers, the high energy intensity and environmental concerns triggered by industrial NF (i.e., the H–B process), the need to develop and integrate more sustainable processes becomes imperative.<sup>[7,8]</sup> Several alternative (non-conventional) technologies are being investigated, such as biological NF,<sup>[9,10]</sup> and NF with metallo-complex homogeneous catalysts under ambient pressure.<sup>[11]</sup> Another new technology considered to have great potential for reducing the environmental impact and improving the energy efficiency is based on plasma, that is, an ionised gas, typically created by applying electric energy. Especially when sustainable energy sources such as wind and solar cells are utilised for the generation of electricity, the dependence on fossil

[a] Dr. W. Wang, S. Heijkers, Prof. Dr. A. Bogaerts  
Department of Chemistry, research group PLASMANT  
University of Antwerp  
Universiteitsplein 1, 2610 Antwerp (Belgium)  
E-mail: wangweizong@gmail.com  
annemie.bogaerts@uantwerpen.be

[b] B. Patil, Prof. Dr. V. Hessel  
Department of Chemical Engineering and Chemistry  
Laboratory of Chemical Reactor Engineering/  
Micro Flow Chemistry and Process Technology  
Eindhoven University of Technology  
P. O. Box 513, 5600 MB Eindhoven (The Netherlands)

Supporting Information and the ORCID identification number(s) for the author(s) of this article can be found under <http://dx.doi.org/10.1002/cssc.201700095>.

fuels during this industrial process is greatly reduced and no greenhouse gas emissions take place. This makes plasma an inherent “green” technology.

Plasma-based NF is generally accomplished by the reaction of nitrogen with oxygen or hydrogen to produce nitrogen oxide (nitric oxide) or ammonia, respectively.<sup>[1]</sup> For plasma-based ammonia synthesis, expensive hydrogen is required in addition to readily available nitrogen. In contrast, for plasma-based nitric oxide synthesis, the raw materials (air) are abundantly available at low cost. As a result, more research devoted to the plasma-based nitric oxide synthesis can be found in the literature.<sup>[12–16]</sup> For this purpose, either thermal or non-thermal plasma can be used. Thermal plasma, however, requires very high temperatures and the energy efficiency is low. Non-thermal plasma, on the other hand, is very promising because the theoretical limit of the energy consumption of nitrogen oxidation is more than 2.5 times lower than that of the H–B process.<sup>[16]</sup> Thus, atmospheric non-thermal plasmas offer unique perspectives because of their capacity to induce chemical reactions within gases with a limited energy cost at ambient pressure and temperature.

Gliding arc plasmas are among the most effective and promising plasmas for gas conversion<sup>[17–30]</sup> because they offer benefits of both thermal and non-thermal discharges. They are typically considered as “warm” discharges, and vibrational excitation of the molecules is seen as the most efficient way to assist the conversion or synthesis.<sup>[31]</sup> A few studies were reported on employing a gliding-arc reactor for NF.<sup>[32–38]</sup> The highest concentration of NO<sub>x</sub> achieved was found to be 1.0% in a mill-scale gliding-arc reactor.<sup>[37]</sup> In this reactor, one can expect to benefit from an intensified contact of the reactive plasma species with the gas molecules, and therefore a higher efficiency in delivering energy to the reactant gases.

To improve the applications (i.e., mainly gas conversion), the physical and chemical characteristics of the gliding arc have been extensively studied experimentally.<sup>[39–44]</sup> Furthermore, computer modelling of the plasma chemistry and reactor design<sup>[45–59]</sup> is also very useful in providing more insight into the underlying reaction mechanisms of plasma-assisted gas conversion or synthesis, for example, by evaluating quantities that are difficult to measure, and by identifying the most important chemical reactions or parameters.<sup>[45–51]</sup> However, only a few papers in literature deal with modelling of a gliding arc.<sup>[52–59]</sup> To our knowledge, there exist no models yet for NO<sub>x</sub> synthesis in a gliding arc.

Previous theoretical analysis revealed that vibrationally excited nitrogen plays an important role in energy efficient NO formation,<sup>[16,38]</sup> but these studies lack a description of the plasma chemistry. For N<sub>2</sub>/O<sub>2</sub> mixtures, several papers presented kinetic models with a complex description of the vibrational and electronic levels,<sup>[60–64]</sup> but these models do not apply to a gliding-arc reactor. As a result, the various mechanisms that contribute to NO<sub>x</sub> production in a gliding arc are not yet completely understood. This may be because a gliding arc is a non-stationary discharge and its effective volume changes due to the arc elongation caused by the gas blast. Therefore, building an ac-

curate model for such a non-uniform reactor with a complex plasma chemistry is very challenging.

Herein, for the first time, we study the NO<sub>x</sub> synthesis in a pulsed-power gliding-arc reactor by a chemical kinetics model. Experiments are performed to benchmark the model. More specifically, we compare the calculated and measured product yields of various NO<sub>x</sub> compounds, the reaction selectivity and energy efficiency for different feed ratios of N<sub>2</sub>/O<sub>2</sub>. Moreover, by comparing these values with those for the pure thermal process, in which most of the energy is spent on the gas heating rather than on the nitrogen oxidation reactions, we can clearly demonstrate the non-equilibrium character of the gliding arc and explain the higher values of the NO<sub>x</sub> yield and energy efficiency. Furthermore, to increase our general understanding of the underlying mechanisms and pathways, we perform a kinetic analysis, based on the simulation results, to elucidate the role of various plasma species, and especially of the N<sub>2</sub> vibrational states, in the NO<sub>x</sub> synthesis. This enables us to propose solutions on how to further improve the formation of NO<sub>x</sub> by gliding arc technology.

## Results and Discussion

### NO<sub>x</sub> formation

The measured and calculated NO and NO<sub>2</sub> concentrations are plotted as a function of N<sub>2</sub>/O<sub>2</sub> ratio in the gas mixture in Figure 1 a,b. The total NO<sub>x</sub> concentration (i.e., sum of NO + NO<sub>2</sub>) and the NO and NO<sub>2</sub> selectivity are presented in Figure 2 a,b.

Note that the experiments are limited to a N<sub>2</sub>/O<sub>2</sub> ratio in the range of 0.25–4, whereas the simulations are performed in a wider range of 0.025–40 to obtain additional information. The concentrations of NO and NO<sub>2</sub> follow a similar parabolic trend upon varying the N<sub>2</sub>/O<sub>2</sub> ratio, and there is an optimum feed ratio at which the maximum yield is reached. This is logical, because both N<sub>2</sub> and O<sub>2</sub> are the (initial) precursors for NO and NO<sub>2</sub>. In the experiment, the concentration of NO increases until a feed ratio of 3 after which the NO concentration starts to decline. The NO<sub>2</sub> concentration reaches its peak at a feed ratio of 1. The calculated results follow a left-skewed trend for both NO and NO<sub>2</sub>, as well as for their sum, with respect to the experimental values. However, the absolute values of the calculated and measured concentrations are in rather good agreement, certainly in view of the complexity of the plasma chemistry.

At a feed ratio of N<sub>2</sub>/O<sub>2</sub> around 1, both the NO and NO<sub>2</sub> selectivity are close to 50%, but at a higher feed ratio, both the experimental and calculated NO selectivity increase, whereas the NO<sub>2</sub> selectivity shows the opposite trend. This is logical, because NO<sub>2</sub> production by NO oxidation becomes less important upon increasing fraction of N<sub>2</sub>. When the feed ratio of N<sub>2</sub>/O<sub>2</sub> is below 1, the NO selectivity again increases slightly, and the calculated value reaches about 60% at a low N<sub>2</sub>/O<sub>2</sub> ratio around 0.02, whereas the calculated NO<sub>2</sub> selectivity is only 40%. This is because the net formation rate of NO<sub>2</sub> decreases more than that of NO with increasing O<sub>2</sub> fraction. In general, we can conclude that reasonable agreement is obtained be-

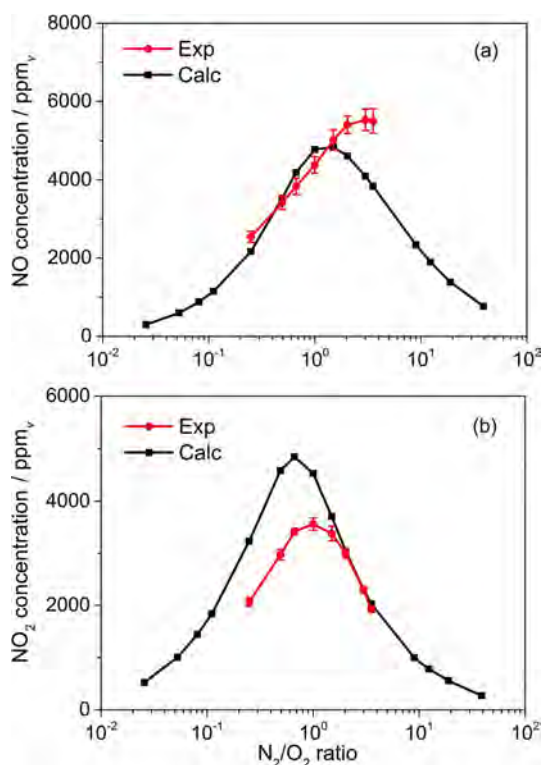


**Figure 1.** Experimental and calculated concentrations of NO (a) and NO<sub>2</sub> (b) as a function of the N<sub>2</sub>/O<sub>2</sub> ratio in the feed gas, for a gas flow rate of 2 L min<sup>-1</sup> and a SEI of 1.4 kJ L<sup>-1</sup> (or 0.35 eV molec<sup>-1</sup>).

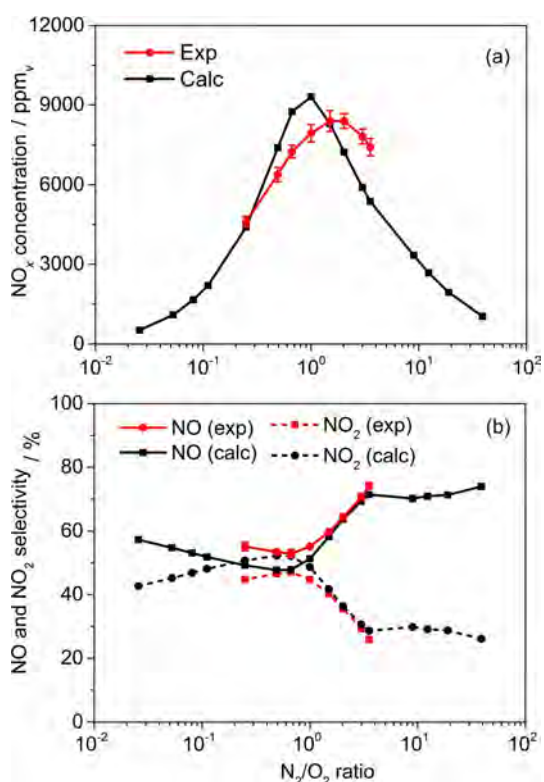


**Figure 2.** Experimental and calculated concentrations of NO<sub>x</sub> (taken as NO + NO<sub>2</sub>) (a) and NO and NO<sub>2</sub> selectivity (b) as a function of the N<sub>2</sub>/O<sub>2</sub> ratio in the feed gas, for a gas flow rate of 2 L min<sup>-1</sup> and a SEI of 1.4 kJ L<sup>-1</sup> (or 0.35 eV molec<sup>-1</sup>).

tween the experimental and calculated data, indicating that the model can provide a more or less realistic picture of the plasma chemistry, and can thus be used to elucidate the underlying mechanisms, as will be shown later.

### Comparison of our results with thermal NO<sub>x</sub> formation and with the H-B process

To evaluate the performance of our gliding arc for NF, we compare our results with the thermal NO<sub>x</sub> yield, calculated as a function of gas temperature (see the calculation method in the Supporting Information). The NO<sub>x</sub> yield calculated by the thermal model is based on the chemical equilibrium composition, which is calculated by finding the composition that minimises the Gibbs free energy. It is a standard technique in equilibrium chemistry and widely used in literature owing to the difficulties in performing experiments at such high temperature.<sup>[65,66]</sup>

Figure 3 shows the calculated equilibrium species composition of a 50% N<sub>2</sub>/50% O<sub>2</sub> mixture, as a function of the gas temperature at atmospheric pressure. At room temperature, the thermal NO<sub>x</sub> (i.e., NO + NO<sub>2</sub>) yield is negligible because the species energy is not high enough to break the nitrogen bond. With increasing gas temperature, the molar fractions of NO and NO<sub>2</sub> increase. The selectivity of NO is higher than that of NO<sub>2</sub> owing to the dissociation of NO<sub>2</sub> into NO and O at higher temperature. The concentration of NO reaches a peak at around 3500 K. A further temperature increase yields a reduction of the NO yield, because of dissociation of NO into N and O atoms.

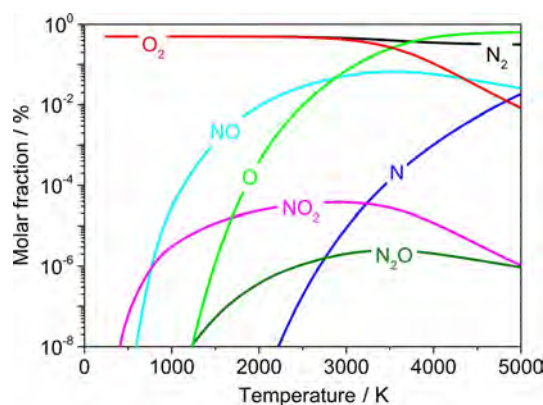


**Figure 3.** Calculated gas composition for a 50% N<sub>2</sub>/50% O<sub>2</sub> mixture, as a function of the gas temperature at atmospheric pressure.

The variations in molar fractions of NO and NO<sub>2</sub> as a function of temperature explain why the thermal NO<sub>x</sub> yield and corresponding energy efficiency both show a peak at a certain temperature, as illustrated in Figure 4. Our calculations predict the highest thermal NO<sub>x</sub> yield of approximately 8% at 3500 K. The corresponding energy efficiency is then about 2.9%. At 3000 K, a somewhat higher energy efficiency of nearly 4% is reached, but the NO<sub>x</sub> yield is then only 5.5%. The reason for reaching a higher energy efficiency at a somewhat lower temperature is



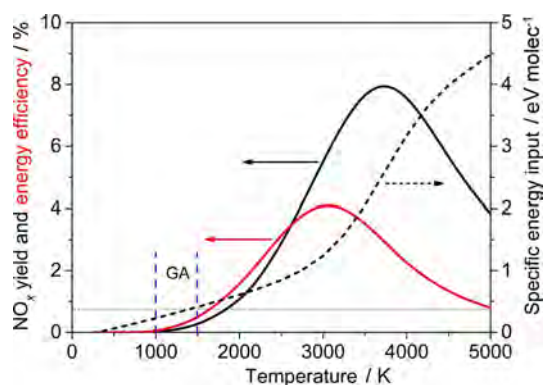


**Figure 4.** Calculated thermal  $\text{NO}_x$  yield (solid black line, left y axis) and corresponding energy efficiency (solid red line, left y axis), as well as the corresponding specific energy input (dashed line, right y axis), as a function of gas temperature for a 50%  $\text{N}_2$ /50%  $\text{O}_2$  mixture at atmospheric pressure. The typical gas temperature range in our gliding arc (GA) is indicated with the blue vertical dashed lines.

simply because a lower specific energy input (SEI) is needed, as seen from the dashed curve in Figure 4; we also indicate the typical gas temperature range in our gliding arc (see the blue vertical dashed lines). The thermal  $\text{NO}_x$  yield is only about 0.16% at 1500 K, which is the highest gas temperature in our gliding arc. Because only a limited fraction (around 7.8%; cf. Supporting Information) of the total gas flowing into the reactor during every gliding-arc cycle is processed by the effective gliding-arc volume ( $v$ ), the thermal  $\text{NO}_x$  yield of 0.16% would correspond to an overall  $\text{NO}_x$  yield of only 25 ppm<sub>v</sub>, which is a factor 320 lower than the value of nearly 8000 ppm<sub>v</sub> that we measured in our gliding arc (cf. Figure 2a). Furthermore, if all the gas flowing into the reactor would be treated by the thermal process, an SEI of 1.4 kJ L<sup>-1</sup> (or 0.35 eV molec<sup>-1</sup>) would lead to an overall  $\text{NO}_x$  yield around 1095 ppm<sub>v</sub>, which is still much lower than our measured value. This low  $\text{NO}_x$  concentration obtained by the thermal process demonstrates that most of the energy is spent on gas heating rather than on nitrogen oxidation, and that our gliding arc clearly operates in non-equilibrium conditions, explaining the much higher  $\text{NO}_x$  yield obtained compared to the thermal process.

The experimental and calculated energy consumption per mole of  $\text{NO}_x$  formed obtained with and without including the energy cost of gas preparation (i.e., air separation) is plotted in Figure 5 as a function of the  $\text{N}_2/\text{O}_2$  ratio. At low  $\text{N}_2/\text{O}_2$  ratios, only considering the plasma energy consumption, the energy required for  $\text{NO}_x$  formation slightly decreases with increasing  $\text{N}_2/\text{O}_2$  ratio, up to a value of 37.1 MJ mol<sup>-1</sup> at a  $\text{N}_2/\text{O}_2$  ratio of 1, after which the experimental value remains constant, whereas the calculated value slightly increases again upon higher  $\text{N}_2/\text{O}_2$  ratios. This is logical because the  $\text{N}_2/\text{O}_2$  ratio around 1 gives rise to the highest calculated  $\text{NO}_x$  concentration. We have also included in Figure 5 the power consumption of  $\text{NO}_x$  formation, accounting for the energy cost of gas preparation (i.e., air separation), in case of a  $\text{N}_2/\text{O}_2$  ratio different from air, and the results show a quite similar trend with variation of the  $\text{N}_2/\text{O}_2$  ratio. The influence of the energy cost of gas preparation on the total energy consumption gradually decreases with in-

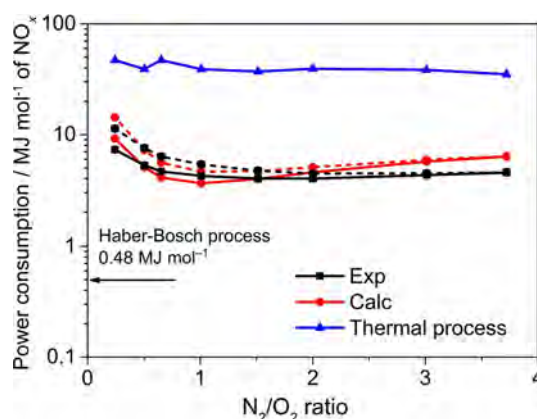


**Figure 5.** Experimental and calculated energy consumption of  $\text{NO}_x$  formation as a function of the  $\text{N}_2/\text{O}_2$  ratio in the mixture, for a gas flow rate of 2 L min<sup>-1</sup> and a SEI of 1.4 kJ L<sup>-1</sup> (or 0.35 eV molec<sup>-1</sup>), and comparison with the thermal process at the same SEI value. The solid and dashed (black and red) lines indicate without and with energy cost of air separation, respectively. The energy consumption of the H-B process is also presented for comparison.

creasing  $\text{N}_2$  content. This is because the pure oxygen flow rate and hence the related energy cost of gas preparation decreases. With a feed ratio of 79%  $\text{N}_2$ /21%  $\text{O}_2$ , air as the only feed gas was found to produce a slightly lower amount of  $\text{NO}_x$  than the mixture with the optimised  $\text{N}_2/\text{O}_2$  feed ratio of around 1.0, for which more energy is needed to prepare pure  $\text{O}_2$  gas and this is definitely beneficial for the costs, yielding a lower total energy consumption, as indicated in Figure 5.

The current industrial-scale H-B process provides a benchmark for the energy consumption for plasma-based NF processes. The energy requirement for the H-B process is much lower, that is, 0.48 MJ mol<sup>-1</sup> of N atoms.<sup>[67]</sup> This value includes the energy consumption during the whole industrial production process of ammonia using three main raw materials: natural gas, air and water. The current comparison indicates that plasma-based NF is not yet competitive with the industrial H-B process, which operates of course on a much larger scale. Hence, it is obvious that much more research is needed to further improve the plasma-based NF process. On the other hand, it is also clear from Figure 5 that the gliding arc requires about 10 times less energy than the thermal process of  $\text{NO}_x$  formation, calculated with the same energy input of 1.4 kJ L<sup>-1</sup> (or 0.35 eV molec<sup>-1</sup>). As the high temperature makes it very challenging to establish a thermal plasma in our gliding-arc reactor, it is difficult to validate our thermal conversion model by direct comparison under specific conditions. However, experimental work in the literature,<sup>[68-72]</sup> performed in other thermal plasma reactors to which our thermal conversion model is applicable, generally yield a higher energy consumption of  $\text{NO}_x$  synthesis than in our current work, because the energy in a thermal system is distributed over all degrees of freedom, including those not effective for the  $\text{NO}_x$  synthesis. This is in reasonable agreement with the prediction of our thermal model, although it is not really possible to compare different reactor setups with different discharge conditions.

The fact that the energy efficiency of the gliding arc for NO<sub>x</sub> synthesis is much better than that for the thermal process can also be deduced from Figure 6. Indeed, both the calculated and measured energy efficiency, with and without considering the energy cost of gas preparation (i.e., air separation), are

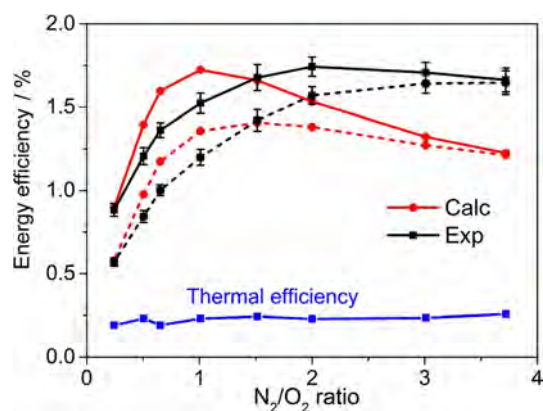
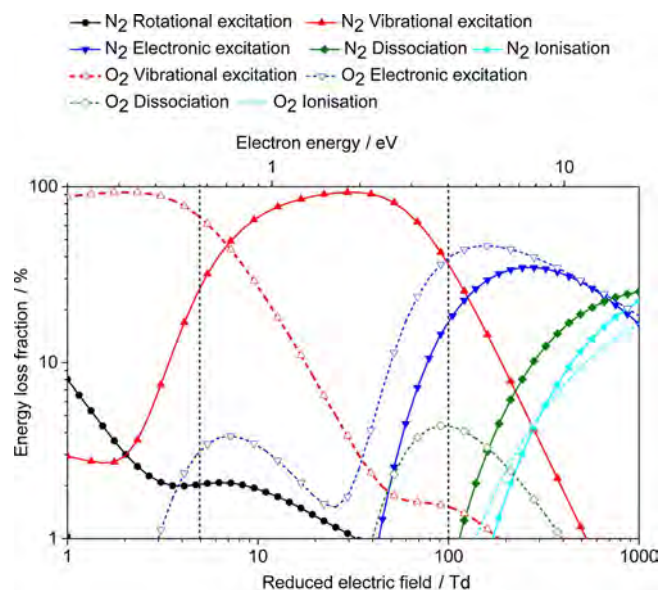


**Figure 6.** Experimental and calculated energy efficiency of NO<sub>x</sub> formation as a function of the N<sub>2</sub>/O<sub>2</sub> ratio in the mixture, for a gas flow rate of 2 L min<sup>-1</sup> and a SEI of 1.4 kJ L<sup>-1</sup> (or 0.35 eV molec<sup>-1</sup>), and comparison with the thermal energy efficiency at the same SEI value. The solid and dashed (black and red) lines indicate without and with the energy cost of air separation, respectively.

around 0.5–1.7%, whereas the thermal energy efficiency calculated for the same SEI of 1.4 kJ L<sup>-1</sup> is only about 0.2%. Hence, this clearly demonstrates the non-equilibrium character of the gliding arc for NO<sub>x</sub> synthesis, that is, the NO<sub>x</sub> synthesis does not proceed thermally but upon electron-induced processes, contributing to energy efficient chemical reactions, as will be explained below. Moreover, when including the energy cost related to the gas preparation (i.e., producing pure O<sub>2</sub> gas from air), the experimental energy efficiency using air (i.e., N<sub>2</sub>/O<sub>2</sub> ratio of 79%:21%) shows the highest value of all different feed ratios, although the addition of oxygen to air slightly enhances the production of NO<sub>x</sub> to some extent. This once again shows that inexpensive and readily available atmospheric pressure air is suited and preferred instead of an artificial N<sub>2</sub>+O<sub>2</sub> mixture.

#### Underlying mechanisms of NO<sub>x</sub> formation in the gliding arc: energy efficient process by vibrational excitation of N<sub>2</sub>

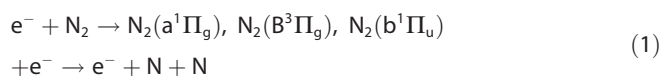
As mentioned above, the NO<sub>x</sub> formation in our gliding arc, as well as in other types of plasmas, is induced by electron impact reactions with the N<sub>2</sub> and O<sub>2</sub> molecules. In Figure 7, we illustrate how the electron energy is transferred to different channels of excitation, ionization and dissociation of both N<sub>2</sub> and O<sub>2</sub> molecules in a 50% N<sub>2</sub>/50% O<sub>2</sub> mixture, as a function of the reduced electric field ( $E/N$ , where  $E$  is electric field and  $N$  is concentration of neutral particles) in the discharge. This reduced electric field is an important parameter to distinguish different plasma types, as it determines the average electron energy in the plasma, and thus the rate of the various electron impact reactions. The electron energy values corresponding to

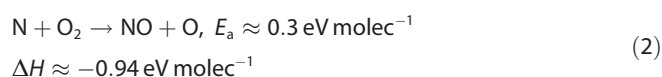


**Figure 7.** Fraction of electron energy transferred to different channels of excitation, as well as ionization and dissociation of N<sub>2</sub> and O<sub>2</sub>, in a 50% N<sub>2</sub>/50% O<sub>2</sub> mixture, as a function of the reduced electric field ( $E/N$ ), as calculated from the corresponding cross sections of the electron impact reactions. The reactions with N<sub>2</sub> are indicated with solid lines, whereas the corresponding reactions with O<sub>2</sub> are plotted with dashed lines. The electron energies corresponding to the reduced electric field values are indicated at the top x axis. The region between the two dashed vertical lines, indicating a reduced electric field between 5 and 100 Td, corresponds to the typical gliding-arc regime.

the reduced electric field values are thus also indicated in Figure 7 (see top and bottom x axes). A gliding arc is typically characterised by reduced electric field values between 5 and 100 Td (see the vertical dashed lines in Figure 7), whereas a dielectric barrier discharge (DBD), which is a quite popular type of plasma for gas conversion applications, typically operates at values higher than 100 Td.<sup>[31]</sup> Note that 1 Td (Townsend) corresponds to 10<sup>-21</sup> V m<sup>-2</sup>.

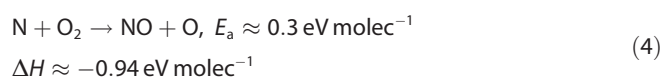
It is known that the energy efficiency of NO<sub>x</sub> formation is determined by the method to break the strong ( $\approx 10$  eV) bond of the N<sub>2</sub> molecule. Above approximately 100 Td, as we can see from Figure 7, most electron energy goes into electronic excitation, dissociation and ionisation of the N<sub>2</sub> (and O<sub>2</sub>) molecules. The N atoms produced by direct electron impact dissociation of N<sub>2</sub> molecules can react with O<sub>2</sub> molecules to form NO. However, owing to the very high dissociation threshold level of N<sub>2</sub>, the energy efficiency in this case would be limited to a low level of about 3%.<sup>[31]</sup> This explains why a DBD is characterised by a lower energy efficiency, or a higher energy consumption for NO<sub>x</sub> synthesis. Indeed, in Ref. [73], an energy consumption of 18.0 MJ mol<sup>-1</sup> was obtained for NO<sub>x</sub> synthesis in a DBD reactor, which is clearly lower than in our case. We can describe this mechanism as follows in Equations (1) and (2):





A similar mechanism, based on electron impact dissociation of  $\text{N}_2$ , was also predicted by our model, and validated by experiments, for a  $\text{CO}_2/\text{N}_2$  mixture in a DBD reactor.<sup>[50]</sup>

On the other hand, in the reduced electric field range lower than 100 Td, which is characteristic for our gliding arc, electron impact vibrational excitation of  $\text{N}_2$  is the dominant electron process, as is clear from Figure 7, and the resulting  $\text{N}_2$  molecules in vibrational levels will be important for NO formation in our case. Indeed, the relatively high energy barrier of the reaction between  $\text{N}_2$  molecules and O atoms to form NO, that is, approximately 3 eV, can be overcome by the vibrational energy of the  $\text{N}_2$  molecules. As a result, the so-called Zeldovich mechanism stimulated by vibrational excitation<sup>[31]</sup> will play the dominant role for producing NO in our gliding arc, whereas the N formed in this process can react with an  $\text{O}_2$  molecule to form another NO [Eqs. (3), (4)]:



(v) indicates in vibrational state. This will be further elaborated in the next section.

To demonstrate that the  $\text{N}_2$  vibrational levels are indeed important in our gliding arc, we plot in Figure 8 the vibrational distribution of  $\text{N}_2$  in the gliding arc at four different times, that is, at 5  $\mu\text{s}$  (corresponding to the beginning of the first pulse; see the Supporting Information for details), 15, 25, and 35  $\mu\text{s}$  (i.e., at the end of the first pulse). At the time instant of 5  $\mu\text{s}$ , mainly the low vibrational levels are populated, owing to electron excitation. When time evolves, the fast vibrational–vibrational (VV) relaxation, which represents the vibrational energy exchange among two molecules in the same mode of vibra-

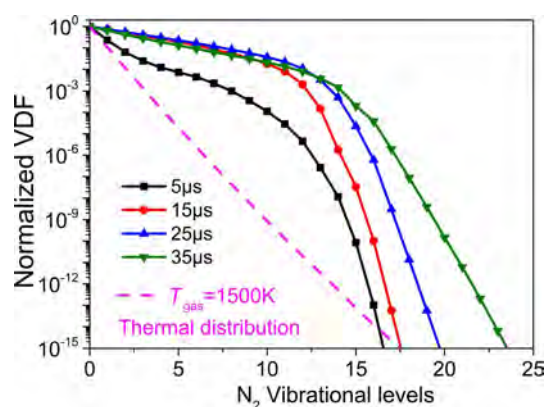


**Figure 8.** Normalised vibrational distribution function at different time instants of the first discharge pulse for a 50%  $\text{N}_2$ /50%  $\text{O}_2$  mixture. The thermal distribution at the gas temperature of 1500 K is also presented for comparison.

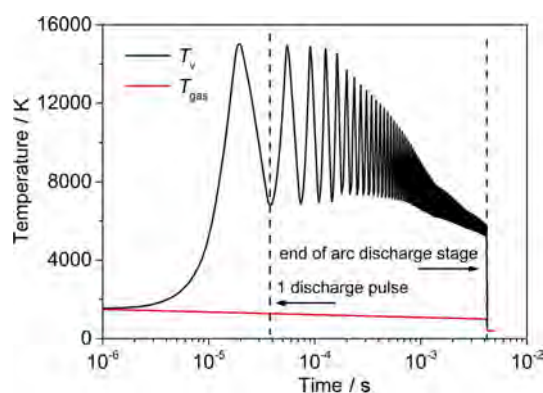
tion, leads to the establishment of a vibrational distribution in which the high-energy levels are also gradually more populated, as is clear from Figure 8. If the vibrational energy lost to translational degrees of freedom (i.e., vibrational–translational (VT) relaxation processes) and chemical reactions would be neglected, the vibrational levels would show a Treanor distribution, that is, an exponentially parabolic distribution function with a minimum value at intermediate vibrational levels.<sup>[74]</sup> However, when the chemical reactions of the vibrational levels are taken into account, the highest vibrational levels can overcome the reaction energy barrier. As a result, the destruction rate of the high vibrational levels is very large and the normalised vibrational distribution function shows a decreasing trend with a larger slope with rising vibrational levels. By comparing the vibrational distribution functions calculated in the gliding arc with the equilibrium thermal distribution, calculated for a gas temperature of 1500 K, which is also plotted in Figure 8, it is obvious that the gliding arc discharge is highly vibrationally overpopulated throughout the entire power deposition pulse (or discharge cycle), explaining the important role of the  $\text{N}_2$  vibrational levels in the NO formation in our gliding arc (see also next section).

Figure 9 illustrates the calculated vibrational temperature of  $\text{N}_2$  as a function of time during the entire gliding-arc discharge stage. It is defined as follows from the first vibrational level [Eq. (5)]:

$$T_v = \frac{E_{v1}}{k_B \ln(n_1/n_0)} \quad (5)$$

where the  $v$  stands for vibrational state  $E_{v1}/k_B = 3481 \text{ K}$  is the energy of  $\text{N}_2(v1)$  and  $n_1$  and  $n_0$  are the densities of  $\text{N}_2(v1)$  and  $\text{N}_2$  ground state, respectively.  $k_B$  is the Boltzmann constant.

In our experiments, we use a high-frequency pulsed power, which leads to oscillations in the power deposition. Therefore, the electron temperature and electron number density also show this oscillation behaviour (see details in the Supporting Information). Hence, it is clear that the vibrational temperature, which is determined by electron impact vibrational excitation, and thus strongly depends on the electron properties (see de-



**Figure 9.** Vibrational temperature of the first vibrational ( $T_v$ ) state of  $\text{N}_2$  as a function of time in the gliding arc discharge for a 50%  $\text{N}_2$ /50%  $\text{O}_2$  mixture. The gas temperature is also presented for comparison.



tails in the Supporting Information), also exhibits the same oscillations, with a peak at maximum power deposition of one discharge pulse, which drops again with the decrease of the power deposition. However, when the power drops to zero, the vibrational temperature is still higher than the gas temperature because it cannot relax back to the gas temperature in the limited timescale before the start of the next power deposition pulse, when the vibrational temperature rises again. The maximum vibrational temperature, however, decreases with time because both the power density and electron number density decrease (see Figure S5 in the Supporting Information), and the electron energy transfer to vibrational energy by electron impact vibrational excitation is thus reduced. Near the end of the arc discharge stage, the vibrational temperature does not show a large variation during and in between two discharge pulses, but it is still considerably higher than the gas temperature (i.e., about 5000 vs. 1000 K), indicating that the vibrational levels are overpopulated during the entire gliding arc cycle, and thus that the gliding arc is far from thermal equilibrium. Our calculated values of the vibrational temperature range from 4500 to 8000 K, which is in general good agreement with experimental investigations<sup>[75,76]</sup> for a kHz alternating current (AC) air gliding arc at atmospheric pressure.

It should be noted that not only the  $N_2$  molecules but also the  $O_2$  molecules are vibrationally excited in the gliding arc. The latter can also help overcome the reaction energy barrier of the NO formation process (see [Eq. (4)] above). However, as we can see from Figure 7, the electron energy is more easily transferred to the vibrational energy of the  $N_2$  molecules in the typical reduced electric field range of a gliding arc. Therefore, we only present here the results of the  $N_2$  vibrational levels. In the next section we will try to elucidate the role of the various plasma chemical reactions and plasma species, and especially of the vibrational levels, on the actual  $NO_x$  synthesis in our gliding-arc reactor.

### Formation and loss processes of NO and $NO_2$

To better understand the influence of the  $N_2/O_2$  feed ratio on the  $NO_x$  yield, we investigated the dominant reaction pathways for the formation and loss of NO and  $NO_2$  for several  $N_2/O_2$  feed ratios. This kinetic analysis was performed by looking at the time and volume integrated rates of the various processes for the total residence time of 5.0 ms (cf. Figure S3 in the Supporting Information).

Table 1 lists the most important formation (F1–F6) and loss (L1–L5) processes for NO. In the Supporting Information (Figure S6) we plot their time and volume integrated rates as a function of  $N_2/O_2$  ratio, as well as the total formation and loss rate. As explained in the Supporting Information, some formation reactions are counteracted by some loss reactions. Hence, to investigate the net contribution of the forward and reverse reactions to the formation of NO, we plot in Figure 10 the time and volume integrated net rates of the various NO formation processes as a function of  $N_2/O_2$  ratio, as well as the total net formation rate.

**Table 1.** Overview of the most important formation and loss reactions for NO.

Formation processes		Loss processes	
F1	$O + N_2(v) \rightarrow NO + N$	L1	$N + NO \rightarrow O + N_2$
F2	$O + NO_2 \rightarrow NO + O_2$	L2	$O + NO \rightarrow NO_2$
F3	$N + O_2/O_2(v) \rightarrow NO + O$	L3	$NO + NO_2 + M \rightarrow N_2O_3 + M$
F4	$N_2O_3 + M \rightarrow NO + NO_2 + M$	L4	$NO_3 + NO \rightarrow NO_2 + NO_2$
F5	$N + NO_2 \rightarrow NO + NO$	L5	$NO_2^- + NO_2 \rightarrow NO_3^- + NO$
F6	$NO_2^- + NO_2 \rightarrow NO_3^- + NO$		

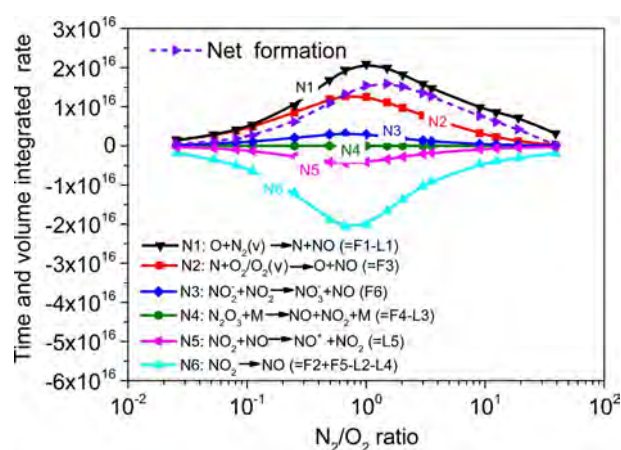


**Figure 10.** Time and volume integrated net rates of the various NO formation processes as a function of  $N_2/O_2$  ratio, for a SEI of  $1.4 \text{ kJ L}^{-1}$  (or  $0.35 \text{ eV molec}^{-1}$ ), as well as the total net formation rate.

Although the collision between oxygen atoms and  $NO_2$  (F2 in Table 1) is the dominant formation mechanism of NO at low  $N_2/O_2$  ratio, or high oxygen contents in the mixture, as shown in Figure S6, the reactions that proceed from  $NO_2$  have an overall negative net contribution to the NO formation, as is obvious from Figure 10 (see N6). This indicates that there is more formation of  $NO_2$  from NO than vice versa, and reaction F2 does not count as net formation process of NO. In contrast, the rate of reaction F1 is 18% higher than the rate of its reverse reaction L1 at the  $N_2/O_2$  feed ratio of 1.0 (see Figure S6), and thus, reaction F1 has a clear net contribution to NO formation (see N1 in Figure 10). From this analysis we can therefore draw the following conclusion: the Zeldovich mechanism stimulated by vibrational excitation (F1 in Table 1) is the dominant production process of NO in the gliding arc, but the NO synthesis could be further enhanced if its reverse reaction (L1) could be reduced. Additionally, the second important formation process of NO is the reaction of N atoms with  $O_2$  molecules (either in ground state or vibrational levels) (F3), so we should aim to steer the N atoms, formed in reaction F1, to react with  $O_2$  molecules in reaction F3, instead of reacting with the NO molecules in the reverse reaction L1, to optimise the NO synthesis.

Table 2 lists the most important formation (F7–F10) and loss (L6–L11) processes for  $NO_2$ . Their time integrated rates are plotted in Figure S7 in the Supporting Information, as a function of  $N_2/O_2$  ratio, as well as the total formation and loss rate.

Formation processes		Loss processes	
F7	O + NO → NO <sub>2</sub>	L6	O + NO <sub>2</sub> → NO + O <sub>2</sub>
F8	N <sub>2</sub> O <sub>4</sub> + M → NO <sub>2</sub> + NO <sub>2</sub> + M	L7	NO <sub>2</sub> + NO <sub>2</sub> + M → N <sub>2</sub> O <sub>4</sub> + M
F9	NO <sub>3</sub> + NO → NO <sub>2</sub> + NO <sub>2</sub>	L8	NO <sub>2</sub> + NO <sub>2</sub> → NO <sub>3</sub> + NO
F10	N <sub>2</sub> O <sub>3</sub> + M → NO + NO <sub>2</sub> + M	L9	NO + NO <sub>2</sub> + M → N <sub>2</sub> O <sub>3</sub> + M
		L10	N + NO <sub>2</sub> → NO + NO
		L11	N + NO <sub>2</sub> → O + N <sub>2</sub> O

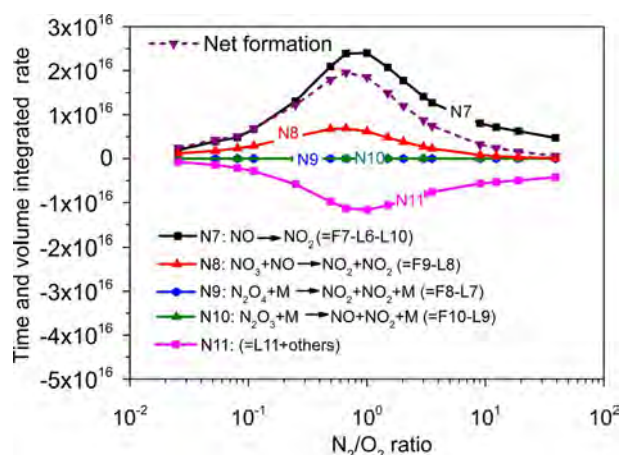


Figure 11. Time and volume integrated net rates of various NO<sub>2</sub> formation processes as a function of N<sub>2</sub>/O<sub>2</sub> ratio, for a SEI of 1.4 kJ L<sup>-1</sup> (or 0.35 eV molec<sup>-1</sup>), as well as the total net formation rate.

Figure 11 shows the time and volume integrated net rates of the various NO<sub>2</sub> formation processes as a function of N<sub>2</sub>/O<sub>2</sub> ratio. Although the reactions involving N<sub>2</sub>O<sub>4</sub>, that is, F8 and L7, are the dominant formation and loss mechanism of NO<sub>2</sub> at N<sub>2</sub>/O<sub>2</sub> feed ratio between 0.2 and 10, as shown in Figure S7 in the Supporting Information, their absolute reaction rates are nearly balanced. Therefore, these reactions (combined as N9) have a negligible net contribution to the formation of NO<sub>2</sub>. The same applies to the reaction N10, involving N<sub>2</sub>O<sub>3</sub> (F10 and L9). Our calculations clearly indicate that the oxidation of NO via F7 is the most important net formation process of NO<sub>2</sub> (N7).

### Overall reaction scheme of the NO<sub>x</sub> chemistry

The data revealed by our 0D model allow us to compose an overall reaction scheme for the NO<sub>x</sub> synthesis, as depicted schematically in Figure 12. The 9.8 eV strong triple bond of N<sub>2</sub> is mainly broken by vibrational excitation, followed by the reaction of N<sub>2</sub>(v) with O atoms into NO and N [Eq. (3)]. The N atoms subsequently react with O<sub>2</sub> molecules to form a second NO and a new O atom [Eq. (4)]. The reaction chain is closed when the new O atom reacts with the next vibrationally excited N<sub>2</sub> molecule. Overall, NO is thus mainly produced by the non-thermal Zeldovich mechanism stimulated by vibrational excitation in the gliding arc. Indeed, the average electron energy in the gliding arc is in the range of 0.6–4.0 eV, which re-

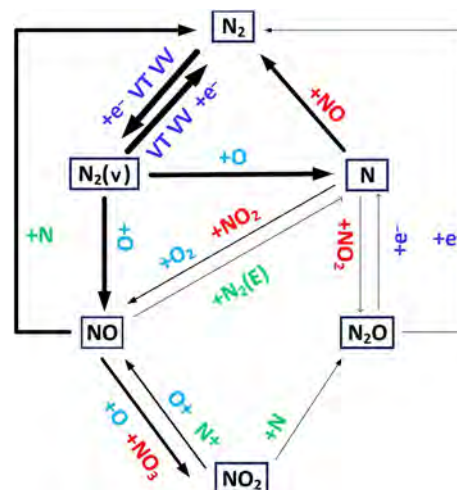


Figure 12. Reaction scheme to illustrate the main pathways of the NO<sub>x</sub> chemistry in the gliding arc as predicted by our model. The thickness of the arrows corresponds to the importance of the reactions for a 50% N<sub>2</sub>/50% O<sub>2</sub> mixture. For instance, the thickness of the arrow from N<sub>2</sub>(v) to NO corresponds to a time and volume integrated rate of 1.37 × 10<sup>17</sup>. N<sub>2</sub>(E) indicates the sum of all the electronically excited N<sub>2</sub> molecules.

sults in about 50–90% electron energy transfer to N<sub>2</sub> vibrational excitation (see Figure 7), whereas VV relaxation further populates the higher N<sub>2</sub> vibrational levels. The latter helps overcome the high reaction energy barrier of the Zeldovich reaction (3 eV molec<sup>-1</sup>) and to promote the production of NO. Therefore, it is crucial to tune the reduced electric field (E/N) in the gliding arc to establish an energy-efficient way of NO production by the non-equilibrium plasma.

Our simulations indicate that for a total gliding arc cycle, a local NO<sub>x</sub> concentration as high as 20% can be reached within the gliding-arc volume. A large fraction of the produced NO is, however, readily destroyed upon impact with N atoms in the active plasma zone (see also Figure 12). By artificially setting the reaction rate of reaction L1 (Table 1) to zero, our model calculations predict a much higher NO yield of 24588 ppm<sub>v</sub> for a N<sub>2</sub>/O<sub>2</sub> feed ratio of 1, which is around 5 times the yield obtained in Figure 1, by taking into account this loss reaction. Consequently, the energy efficiency will also increase by a factor around 5. This clearly shows that suppressing the loss processes of reaction L1 will enhance the NO<sub>x</sub> yield and hence the overall energy efficiency. The reverse reaction L1 indeed competes with the propagation (reaction F3 in Table 1) of the Zeldovich chain, and it is able to terminate the chain when the NO concentration becomes high in the active discharge zone. This seriously restricts the yield of NO synthesis in our gliding arc. As a result, we should look for ways of suppressing the reverse reaction L1 or promoting the reaction F3, to increase the NO yield and hence improve the energy efficiency. For example, at a fixed SEI, by increasing the gas flow rate, the gas velocity becomes larger than the arc velocity and a larger amount of feed gas will be exposed to the plasma. The local NO concentration inside the arc would then decrease, but the overall NO yield and hence the energy efficiency would rise. Our experimental results for the NO<sub>x</sub> con-

centration versus SEI indeed show that higher flow rates can produce higher  $\text{NO}_x$  concentrations at a fixed SEI. This shows the high potential of the gliding arc discharge for  $\text{NO}_x$  production at higher flow rates.

The promotion of the reaction F3 can be reached when making use of hot N atoms. Indeed, the vibrational energy of  $\text{N}_2(v)$  is higher than the activation energy of the reaction F1 (i.e., 3.0 eV) for vibrational levels above  $v_{12}$ , which corresponds to a vibrational energy of 3.2 eV. Thus, a fraction of the vibrational energy released goes into translational energy of the N atoms (so-called hot N atoms) and assists in the reaction F3, by increasing the rate coefficient of this reaction, and therefore, the NO yield can be enhanced. It is shown in Ref. [77] that increasing the oxygen content in the mixture can help to enhance this effect and promote the reaction F3.

Our reaction scheme (Figure 12) also shows that  $\text{NO}_2$  is mainly formed by oxidation of NO upon reaction with O atoms, whereas it mainly reacts back into NO upon reaction with either O or N atoms, at high or low oxygen contents, respectively. The main channel responsible for the formation of O atoms, which are important to initiate the Zeldovich mechanism via reaction F3, is electron-impact dissociation of  $\text{O}_2$  molecules.

Because the N atoms are lost rapidly via reaction L1, as well as by reactions with  $\text{NO}_2$ , our calculations indicate that the overall N concentration is never more than 0.1%. For this reason,  $\text{N}_2\text{O}$ , which is mainly produced upon reaction between N atoms and  $\text{NO}_2$  (reaction L11 in Table 2), has only a minor concentration in the whole gliding-arc cycle compared with NO and  $\text{NO}_2$ . This is in qualitative agreement with our experiments, as no  $\text{N}_2\text{O}$  was detected.

As mentioned above, the industrial scale H–B process still has a lower energy consumption, that is,  $0.48 \text{ MJ mol}^{-1} \text{ N}$ , so it is clear that major efforts should be taken in gliding arc plasma-based NF to further increase the yield and decrease the energy consumption, to become competitive with the industrial scale H–B process. Computer simulations, as presented here, can help to improve the process, as they elucidate the limiting factors for energy-efficient  $\text{NO}_x$  synthesis, and thus can help provide solutions to overcome these limitations.

On the other hand, it is important to realise that more and more electrical energy nowadays is produced from renewable energy sources (wind or solar), and this trend will continue in the coming years. As renewable energy sources often suffer from fluctuating peak powers (e.g., on windy or sunny days) when the electricity is in principle “for free”, our high-frequency pulsed gliding arc plasma can be very useful for peak shaving, as it is very flexible and can be switched on and off easily, so we expect that it will be very suitable for NF by  $\text{NO}_x$  synthesis using renewable energy. Furthermore, as an instantaneous “on-and-off” technique, the gliding-arc-based NF can be stopped and started more easily than the H–B process, making it possible for farmers in remote locations to locally generate the necessary nitrogenous fertilisers out of “thin air” just using small-scale plants. This application of gliding-arc technology is very promising, especially in regions where a wealth of under-used wind and solar resources exist, which offer farmers a new

source of revenue from their land—a renewable alternative to conventional nitrogenous fertilisers that is compatible with growing crops because of its high operation flexibility.

## Conclusions

The purpose of this work was to obtain a better understanding of the nitrogen fixation (NF) process through  $\text{NO}_x$  synthesis in gliding arc plasma, by means of combined experiments and a zero-dimensional kinetics model. We compared our experimental data with the model predictions and obtained reasonable agreement for the NO,  $\text{NO}_2$ , and total  $\text{NO}_x$  yield, the NO and  $\text{NO}_2$  selectivity, the energy consumption and energy efficiency for the entire range of  $\text{N}_2/\text{O}_2$  feed ratios in the mixture. This indicates that our model can provide a realistic picture of the plasma chemistry and can be used to elucidate the dominant reaction pathways for the  $\text{NO}_x$  synthesis.

Our study clearly reveals that vibrational excitation of  $\text{N}_2$  can help overcome the reaction energy barrier of the non-thermal Zeldovich mechanism:  $\text{O} + \text{N}_2(v) \rightarrow \text{NO} + \text{N}$ , and can thus significantly enhance the production of NO. This provides an energy efficient pathway for NO formation in the gliding arc. Furthermore, our simulation shows that the most important reaction for  $\text{NO}_2$  formation is oxidation of NO by O atoms:  $\text{O} + \text{NO} \rightarrow \text{NO}_2$ .

We also compared our results with those of thermal  $\text{NO}_x$  synthesis. The  $\text{NO}_x$  yield and energy efficiency obtained in our gliding arc are much higher than the thermal values owing to the non-equilibrium properties of the plasma, as the chemistry of the conversion process is induced by energetic electrons. We can conclude that the gliding arc is a very promising candidate for potential industrial scale NF, but the energy consumption achieved in this study is still much higher than the benchmark, that is, the industrial Haber–Bosch process. Therefore, it is clear that the  $\text{NO}_x$  synthesis in the gliding arc should be further improved, for example, by operating at conditions in which the reverse reaction  $\text{N} + \text{NO} \rightarrow \text{O} + \text{N}_2$  is suppressed or where the reaction  $\text{N} + \text{O}_2/\text{O}_2(v) \rightarrow \text{NO} + \text{O}$  is promoted, as our simulations indicate that these processes currently limit the  $\text{NO}_x$  formation.

In general our model allows us to gain better insights into the entire process of  $\text{NO}_x$  formation, which enables us to propose solutions for improving the gliding-arc-based  $\text{NO}_x$  synthesis processes in the future. One example could be to actively tune the reduced electric field (i.e.,  $E/N$  ratio) by optimizing the reactor electrical operational parameters, to promote the vibrational excitation and selectively deliver energy to the Zeldovich chemical reaction of NO synthesis by an energy efficient way. Another example could be to improve the reactor geometry and optimise the flow conditions to expose the maximum amount of feed gas to the gliding arc.

It is clear that NF in the gliding arc is still far from competitive with the world-scale business case of the Haber–Bosch process, but if electricity from sustainable energy sources can be used, the intrinsic potential of gliding-arc-based NF can provide a promising opportunity of producing fertiliser in remote locations. This comes up with realistic scenarios of en-



tering a cutting-edge innovation in new business cases of plasma agriculture.

Furthermore, for practical applications, it would be beneficial to make use of air, which includes a certain amount of humidity. Electric discharges in humid air have been studied already in literature; they produce more reactive species and present highly acid and oxidizing properties towards aqueous solutes.<sup>[78]</sup> These chemical effects can be used for various practical applications, for example, the removal of major pollutants from waste waters.<sup>[79]</sup> However, the interaction mechanism of water vapour with air (N<sub>2</sub>/O<sub>2</sub>) is not yet precisely clarified. Our current work shows that the NO<sub>x</sub> formation by the gliding arc operating in dehumidified air strongly depends on the composition of the feed gas, in which the nature of the interactions, such as vibrational molecular excitation between the constituents, is very important. Therefore, identifying the role of different species, and especially their excited states, and clarifying the underlying chemistry in humid air, for different degrees of humidity, will be of great interest to investigate how to enhance nitrate formation in a humid air gliding arc. This is planned for our future work.

## Experimental Section

### Experimental studies

The experiments were performed at atmospheric pressure in a milli-scale gliding-arc reactor. This is a two-dimensional flat reactor in which the gas flow enters through a nozzle at the bottom of the reactor (see Figure 13a). The reactor consists of two thin diverging knife-shaped molybdenum electrodes with thickness of 1.0 mm and height of 195 mm. The width of the reactor is 135 mm with narrowest discharge gap of 1.3 mm. A schematic diagram of the experimental set-up with milli-scale gliding-arc reactor is also shown in Figure 13b. One of the electrodes is connected to the high-voltage source and the other electrode is grounded. The reactor is powered by a customised Xenionik EP 4000 AC power supply. The applied high voltage and current were measured by a high voltage probe (Tektronix P6015A) and a current sense resistor of 5 Ω, respectively. All electrical signals were recorded using a USB powered four-channel PC oscilloscope (PicoScope R 3000).

Air and O<sub>2</sub> (Linde Gas, 99.9%) were fed into the reactor using mass flow controllers (Bronkhorst) and no pre-heating of the gas occurred. The products were analysed using a Fourier Transform Infrared Spectrophotometer (SHIMADZU, IRTracer-100) at a resolution of 0.5 cm<sup>-1</sup> and the gas cell was equipped with CaF<sub>2</sub> windows (Specac, Storm Series). NO and NO<sub>2</sub> were the only products detected and their concentrations were determined from the adsorption bands at 1900 and 1630 cm<sup>-1</sup>, respectively, using a series of calibration gas mixtures. The reported NO and NO<sub>2</sub> selectivity was calculated using Equations (6) and (7):

$$\text{NO selectivity} = \frac{\text{NO concentration}}{\text{concentration of (NO + NO}_2\text{)}} \quad (6)$$

$$\text{NO}_2 \text{ selectivity} = \frac{\text{NO}_2 \text{ concentration}}{\text{concentration of (NO + NO}_2\text{)}} \quad (7)$$

The arc dynamics in the plasma reactor was obtained using high-speed imaging. This helped us to compute the gliding arc lifetime,

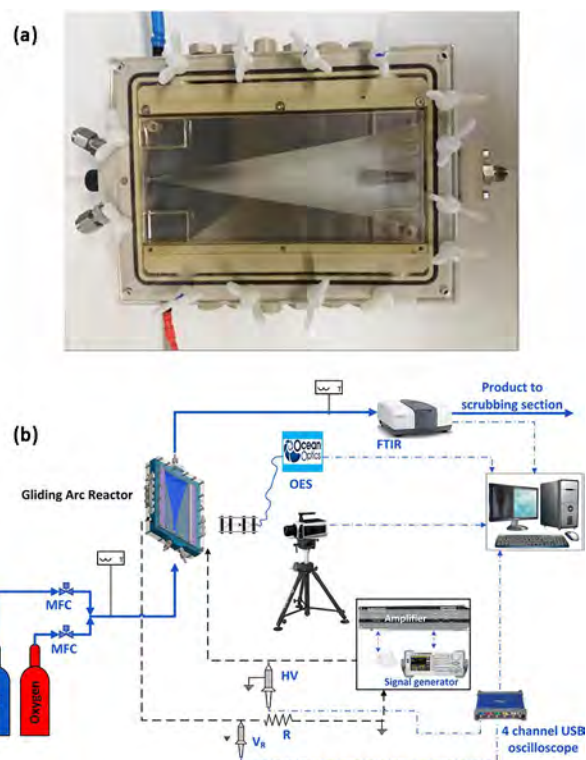


**Figure 13.** Reactor geometry (a) and schematic diagram of the experimental setup (b).

velocity, propagation height and processing time, all of which were used as input in the model (see the Supporting Information). The performance of the milli-scale gliding-arc reactor was investigated at a constant flow rate of 2 L min<sup>-1</sup>, pulse width (25 μs) and amplitude (70 Vpk-pk (peak-to-peak voltage)), and by varying the feed ratio of Air/O<sub>2</sub>, yielding N<sub>2</sub>/O<sub>2</sub> ratios of 0.25–4. All experiments were performed four times and averages of at least 100 voltage-current (*V*–*I*) cycles were used to obtain the final power consumption value. The experiments were reproducible within +/– 5% of the averaged values. The error bars in Figures 1, 2, 5 and 6 show the 95% confidence interval. The influence of different flow rates, pulse widths and amplitudes on the NO<sub>x</sub> yields was investigated in previous work<sup>[37]</sup> and is beyond the scope of our current work. We tested that Air+O<sub>2</sub> and N<sub>2</sub>+O<sub>2</sub> feed gas mixtures with the same ratio of N<sub>2</sub>/O<sub>2</sub> gave very similar concentrations of NO<sub>x</sub> as well as selectivity towards NO, indicating that the minor components in air, such as argon and carbon dioxide, have limited influence on the NO<sub>x</sub> (i.e., NO+NO<sub>2</sub>) yield.<sup>[80]</sup> Therefore, for simplicity, we assumed the air is composed of N<sub>2</sub>/O<sub>2</sub>=79:21 in our simulation mentioned below.

The total plasma power (*P*<sub>plasma</sub>), specific energy input (SEI), and energy consumption (EC) per mole of NO<sub>x</sub> are defined by Equations (8)–(10), respectively (GA: gliding arc).

$$P_{\text{plasma}} (\text{W}) = f \int_0^{t=f_{\text{pulse}}} V_{\text{GA}} \times I_{\text{GA}} dt \quad (8)$$

$$\text{SEI} [\text{J L}^{-1}] = \frac{P_{\text{plasma}} \times 60 [\text{s min}^{-1}]}{\text{gas feed flow rate} [\text{L min}^{-1}]} \quad (9)$$

$$\text{EC} [\text{J mol}^{-1}] = \frac{P_{\text{plasma}} + P_{\text{gp}}}{\text{moles of NO}_x \text{ produced per second}} \quad (10)$$

where  $t_{\text{pulse}}$  is the time span of a pulse (s) and  $f$  is the frequency of the pulses (Hz).  $P_{\text{gp}}$  (W) is the power consumption used to prepare pure oxygen gas from the air by separation [Eq. (11)]:

$$P_{\text{gp}} = \frac{\text{O}_2 \text{ flow rate [L min}^{-1}] \times \text{O}_2 \text{ specific power to separate air [W L}^{-1}]}{60 [\text{s min}^{-1}]} \quad (11)$$

where oxygen specific power for air separation is the power needed to produce a standard litre oxygen gas; a value of 0.28 kW L<sup>-1</sup> is used here, based on Ref. [81].

Likewise, the energy efficiency,  $\eta$ , is calculated as [Eq. (12)]:

$$\eta[\%] = \frac{H_{\text{NO}_x} \times \text{moles of NO}_x \text{ produced per second}}{P_{\text{plasma}} + P_{\text{gp}}} \quad (12)$$

where  $H_{\text{NO}_x}$  [J mol<sup>-1</sup>] is the standard formation enthalpy of 1 mol NO<sub>x</sub>, which is evaluated by Equation (13):

$$H_{\text{NO}_x} = H_{\text{NO}} \times S_{\text{NO}} + H_{\text{NO}_2} \times S_{\text{NO}_2} \quad (13)$$

Where  $H_{\text{NO}}$  and  $H_{\text{NO}_2}$  is the standard formation enthalpy of 1 mol NO (90.3 kJ mol<sup>-1</sup>) and NO<sub>2</sub> (33.1 kJ mol<sup>-1</sup>), respectively, and  $S_{\text{NO}}$  and  $S_{\text{NO}_2}$  is the selectivity of formed NO and NO<sub>2</sub> in the NO<sub>x</sub> products.

## Computational studies

### 0D chemical kinetics model

To elucidate the underlying mechanisms of the gliding arc assisted NO<sub>x</sub> synthesis in the above-mentioned experimental setup, we developed a 0D plasma chemistry model, which allows to describe the behavior of a large number of species, and incorporate a large number of chemical reactions, with limited computational effort.

The zero-dimensional (0D) chemical kinetics model is based on solving balance equations for all the species densities, based on production and loss rates, as defined by the chemical reactions:

$$\frac{dn_i}{dt} = \sum_j \left\{ (a_{ij}^{(2)} - a_{ij}^{(1)}) k_j \prod_i n_i^{a_{ij}^{(1)}} \right\} \quad (14)$$

Where  $a_{ij}^{(1)}$  and  $a_{ij}^{(2)}$  are the stoichiometric coefficients of species  $i$ , at the left and right hand side of a reaction  $j$ , respectively,  $n_i$  is the species density at the left-hand side of the reaction, and  $k_j$  is the rate coefficient of reaction  $j$ . Transport processes such as diffusion are not considered; hence, the species densities are assumed to be constant in the entire simulation volume but they change with

time. Nevertheless, this 0D model allows to describe the spatial dependence of the NO<sub>x</sub> synthesis in the gliding-arc reactor, as explained in the Supporting Information.

The solution of the ordinary differential [Eq. (14)] for the various plasma species is coupled with the Boltzmann equation, which is solved for the electron energy distribution function (EEDF). We use an existing code ZDPlasKin,<sup>[82]</sup> which features an interface for the description of the plasma species and reactions, a solver for the set of differential [Eq. (14)], and an integrated Boltzmann equation solver BOLSIG+.<sup>[83]</sup>

### Plasma chemistry included in the model

The species taken into account in our model for the N<sub>2</sub>/O<sub>2</sub> mixture are listed in Table 3. These species include various neutral molecules in the ground state, as well as several electronically and vibrationally excited levels, various radicals, positive and negative ions, and the electrons.

We pay special attention to the electronically and vibrationally excited states of N<sub>2</sub> and O<sub>2</sub>, because they may become important under certain conditions. The detailed notations of the N<sub>2</sub> electronically excited levels are given in the table, while the vibrational levels of both N<sub>2</sub> and O<sub>2</sub> are indicated with (v). 15 vibrational levels are taken into account for O<sub>2</sub>, while for N<sub>2</sub>, 25 vibrationally excited levels are included. The populations of the higher levels are negligible, as was demonstrated in Figure 8.

All these species undergo a large number of chemical reactions, that is, electron impact collisions with neutral species, leading to excitation, ionization, dissociation and electron attachment, electron-ion recombination reactions, as well as many heavy-particle chemical reactions (i.e., ion-ion, ion-neutral and neutral-neutral reactions).

The chemistry set used in this model is mostly based on the models recently developed within our group, and validated for a microwave discharge<sup>[49]</sup> and a DBD discharge<sup>[50]</sup> in a CO<sub>2</sub>/N<sub>2</sub> mixture. The corresponding rate coefficients, and the references where these data were adopted from, are listed in the Supporting Information of the previous work.<sup>[49]</sup> Some adjustments to the major neutral reactions involving NO<sub>x</sub> were made and their corresponding rate constants are listed in Table 4. The first and fifth reaction do not only apply to N<sub>2</sub> and O<sub>2</sub> molecules in the ground state, respectively, but also to vibrational levels, with the rate coefficients adapted, as elaborated in the supporting information.

Because the vibrational energy can help overcome the activation energy barrier of the reaction and thus increase the reaction rate constant, we present in the supporting information in detail the reactions of the vibrational levels, that is, electron impact excitation, vibrational energy exchange (VT and VV relaxation) reactions and chemical reactions (see section 1: Treatment of the vibrational level in the Supporting Information).

**Table 3.** List of species included in the model for the N<sub>2</sub>/O<sub>2</sub> gas mixture.

Ground neutral species	Charged species	Excited species
N <sub>2</sub> , N	N <sup>+</sup> , N <sub>2</sub> <sup>+</sup> , N <sub>3</sub> <sup>+</sup> , N <sub>4</sub> <sup>+</sup>	N <sub>2</sub> (A <sup>3</sup> Σ <sub>u</sub> <sup>+</sup> ), N <sub>2</sub> (B <sup>3</sup> Π <sub>g</sub> ), N <sub>2</sub> (W <sup>3</sup> Δ <sub>u</sub> ), N <sub>2</sub> (B' <sup>3</sup> Σ <sub>u</sub> <sup>-</sup> ), N <sub>2</sub> (C <sup>3</sup> Π <sub>u</sub> ), N <sub>2</sub> (E <sup>3</sup> Σ <sub>g</sub> <sup>+</sup> ), N <sub>2</sub> (a' <sup>1</sup> Σ <sub>u</sub> <sup>-</sup> ), N <sub>2</sub> (a <sup>1</sup> Π <sub>g</sub> ), N <sub>2</sub> (a'' <sup>1</sup> Σ <sub>g</sub> <sup>+</sup> ), N <sub>2</sub> (w <sup>1</sup> Δ <sub>u</sub> ), N <sub>2</sub> (V1-V25), N(2D), N(2P)
O <sub>2</sub> , O <sub>3</sub> , O N <sub>2</sub> O, N <sub>2</sub> O <sub>4</sub> , N <sub>2</sub> O <sub>5</sub> , NO, NO <sub>2</sub> , NO <sub>3</sub>	O <sup>+</sup> , O <sub>2</sub> <sup>+</sup> , O <sub>4</sub> <sup>+</sup> , O <sup>-</sup> , O <sub>2</sub> <sup>-</sup> , O <sub>3</sub> <sup>-</sup> , O <sub>4</sub> <sup>-</sup> NO <sup>+</sup> , N <sub>2</sub> O <sup>+</sup> , NO <sub>2</sub> <sup>+</sup> , NO <sup>-</sup> , N <sub>2</sub> O <sup>-</sup> , NO <sub>2</sub> <sup>-</sup> , NO <sub>3</sub> , O <sub>2</sub> <sup>+</sup> N <sub>2</sub> electrons (e <sup>-</sup> )	O <sub>2</sub> (V1-V15), O <sub>2</sub> (E1) <sup>[a]</sup> , O <sub>2</sub> (E2) <sup>[b]</sup>

[a] O<sub>2</sub>(E1) = sum of the A<sup>1</sup>Δ and b<sup>1</sup>Σ states. [b] O<sub>2</sub>(E2) = O<sub>2</sub>(B<sup>3</sup>Σ) and higher triplet states.

**Table 4.** Major neutral reactions included in the model.

Reaction	Rate coefficient <sup>[a]</sup>	Ref.
$O + N_2 \rightarrow NO + N$	$3.0 \times 10^{-10} \exp(-38370/T_{\text{gas}})$	[61]
$O + NO_2 \rightarrow NO + O_2$	$6.51 \times 10^{-12} \exp(120.03/T_{\text{gas}})$	[84]
$N + NO \rightarrow O + N_2$	$8.20 \times 10^{-11} \exp(-410.03/T_{\text{gas}})$	[85]
$O + NO \rightarrow NO_2$	$3.02 \times 10^{-11} \exp(T_{\text{gas}}/298.0)^{-0.75}$	[84]
$N + O_2 \rightarrow NO + O$	$4.47 \times 10^{-12} (T_{\text{gas}}/300) \exp(-3270.0/T_{\text{gas}})$	[86]
$NO_3 + NO \rightarrow NO_2 + NO_2$	$1.70 \times 10^{-11}$	[64]
$N + NO_2 \rightarrow NO + NO$	$2.30 \times 10^{-12}$	[64]
$N + NO_2 \rightarrow O + N_2O$	$1.40 \times 10^{-12}$	[85]
$NO_2 + NO_2 \rightarrow NO_3 + NO$	$4.5 \times 10^{-10} \exp(-18500.0/T_{\text{gas}})$	[61]

[a] Rate coefficients are in  $\text{cm}^3 \text{s}^{-1}$  or in  $\text{cm}^6 \text{s}^{-1}$  for the two-body and three-body reactions, respectively;  $T_{\text{gas}}$  is the gas temperature in K.

## Acknowledgements

This research was supported by the European Marie Skłodowska-Curie Individual Fellowship "GlidArc" within Horizon 2020 (Grant No.657304), by the FWO project (grant G.0383.16 N) and by the EU project MAPSYN: Microwave, Acoustic and Plasma assisted SYNthesis, under the grant agreement no. CP-IP 309376 of the European Community's Seventh Framework Program. The calculations were performed using the Turing HPC infrastructure at the CalcUA core facility of the Universiteit Antwerpen (UAntwerpen), a division of the Flemish Supercomputer Center VSC, funded by the Hercules Foundation, the Flemish Government (department EWI) and the UAntwerpen.

## Conflict of interest

The authors declare no conflict of interest.

**Keywords:** energy efficiency · gliding arc · nitrogen fixation · nitrogen oxide · plasma chemistry

- [1] B. S. Patil, Q. Wang, V. Hessel, Jüergen. Lang, *Catal. Today* **2015**, *256*, 49–66.
- [2] N. Cherkasov, A. O. Ibhaddon, P. Fitzpatrick, *Chem. Eng. Process.* **2015**, *90*, 24–33.
- [3] <http://energy.globaldata.com/media-center/press-releases/oil-and-gas/global-ammonia-capacity-to-reach-almost-250-million-tons-per-year-by-2018-says-globaldata>.
- [4] J. N. Galloway, *Environ. Pollut.* **1998**, *102*, 15–24.
- [5] Y. Tanabe, Y. Nishibayashi, *Coord. Chem. Rev.* **2013**, *257*, 2551–2564.
- [6] R. R. Schrock, *Proc. Natl. Acad. Sci. USA* **2006**, *103*, 17087.
- [7] A. Anastasopoulou, Q. Wang, V. Hessel, J. Lang, *Processes* **2014**, *2*, 694–710.
- [8] V. Hessel, G. Cravotto, P. Fitzpatrick, B. S. Patil, J. Lang, W. Bonrath, *Chem. Eng. Process.* **2013**, *71*, 19–30.
- [9] R. H. Burris, G. P. Roberts, *Annu. Rev. Nutr.* **1993**, *13*, 317–335.
- [10] T. Bazhenova, A. Shilov, *Coord. Chem. Rev.* **1995**, *144*, 69–145.
- [11] M. E. Vol'pin, V. B. Shur, M. A. Ilatovskaya, *Bull. Acad. Sci. USSR Div. Chem. Sci.* **1964**, *13*, 1644.
- [12] D. Rapakoulias, S. Cavadias, J. Amouroux, *Revue de Physique Appliquée (Paris)* **1980**, *15*, 1261–1265.
- [13] I. Pollo, *Biul. Lubel. Tow. Nauk. Mat.-Fiz.-Chem.* **1978**, *20*, 102–108.
- [14] J. Krop, I. Pollo, *Chemia* **1980**, *633*, 25–33.
- [15] V. Mutel, O. Dessaux, P. Goudmand, *Rev. Phys. Appl.* **1984**, *19*, 461–464.
- [16] V. D. Rusanov, A. A. Fridman, G. V. Sholin, *Sov. Phys. Usp.* **1981**, *24*, 447–474.

- [17] A. Czernichowski, *Pure Appl. Chem.* **1994**, *66*, 1301–1310.
- [18] A. Indarto, D. R. Yang, J. W. Choi, H. Lee, H. K. Song, *J. Hazard. Mater.* **2007**, *146*, 309–315.
- [19] T. Nunnally, K. Gutsol, A. Rabinovich, A. Fridman, A. Gutsol, A. Kemoun, *J. Phys. D* **2011**, *44*, 274009.
- [20] X. Tao, M. Bai, X. Li, H. Long, S. Shang, Y. Yin, X. Dai, *Prog. Energy Combust. Sci.* **2011**, *37*, 113–124.
- [21] G. Petitpas, J. D. Rollier, A. Darmon, J. Gonzalez-Aguilar, R. Metkemeijer, L. Fulcheri, *Int. J. Hydrogen Energy* **2007**, *32*, 2848–2867.
- [22] C. S. Kalra, A. F. Gutsol, A. A. Fridman, *IEEE Trans. Plasma Sci.* **2005**, *33*, 32–41.
- [23] T. Sreethawong, P. Thakonpatthanakun, S. Chavadej, *Int. J. Hydrogen Energy* **2007**, *32*, 1067–1079.
- [24] Y. N. Chun, H. O. Song, *Energy Sources. A* **2008**, *30*, 1202–1212.
- [25] H. Zhang, F. Zhu, X. D. Li, K. F. Cen, C. M. Du, X. Tu, *Plasma Chem. Plasma Process.* **2016**, *36*, 813–834.
- [26] D. R. Yang, J. W. Choi, H. Lee, H. K. Song, *J. Hazard. Mater.* **2007**, *146*, 1–11.
- [27] S. C. Kim, M. S. Lim, Y. N. Chum, *Plasma Chem. Plasma Process.* **2014**, *34*, 125–143.
- [28] H. Zhang, X. D. Li, F. S. Zhu, K. F. Cen, C. M. Du, X. Tu, *Chem. Eng. J.* **2017**, *310*, 114–119.
- [29] H. Zhang, C. M. Du, A. J. Wu, Z. Bo, J. H. Yan, X. D. Li, *Int. J. Hydrogen Energy* **2014**, *39*, 12620–12635.
- [30] A. A. Fridman, S. Nester, L. A. Kennedy, A. Saveliev, O. Mutaf-Yardimci, *Prog. Energy Combust. Sci.* **1999**, *25*, 211–231.
- [31] A. Fridman, *Plasma Chemistry*, Cambridge University Press, New York, **2008**.
- [32] R. Burlica, M. J. Kirkpatrick, B. R. Locke, *J. Electrostat.* **2006**, *64*, 35–43.
- [33] J. M. Cormier, O. Aubry, A. Khacef, in *NATO Science for Peace and Security Series A: Chemistry and Biology* (Eds.: S. Gucer, A. Fridman) Springer, Netherlands, **2008**, pp. 125–134.
- [34] Z. Czekalska, *Arch. Combust.* **2010**, *30*, 337–346.
- [35] Z. Bo, J. Yan, X. D. Li, Y. Chi, K. F. Cen, *J. Hazard. Mater.* **2009**, *166*, 1210–1216.
- [36] J. Yang, T. Y. Lia, C. S. Zhong, X. X. Guan, C. Hu, *J. Electrochem. Soc.* **2016**, *163*, E288–E292.
- [37] B. S. Patil, J. R. Palau, V. Hessel, J. Lang, Q. Wang, *Plasma Chem. Plasma Process.* **2016**, *36*, 241–257.
- [38] J. Amouroux, S. Cavadias, D. Rapakoulias, *Rev. Phys. Appl.* **1979**, *14*, 969–976.
- [39] X. Tu, H. J. Gallon, J. C. Whitehead, *IEEE Trans. Plasma Sci.* **2011**, *39*, 2900–2901.
- [40] X. Tu, J. C. Whitehead, *Int. J. Hydrogen Energy* **2014**, *39*, 9658–9669.
- [41] S. Pellerin, J. M. Cormier, F. Richard, K. Musiol, J. Chapelle, *J. Phys. D* **1999**, *32*, 891–897.
- [42] I. V. Kuznetsova, N. Y. Kalashnikov, A. F. Gutsol, A. A. Fridman, L. A. Kennedy, *J. Appl. Phys.* **2002**, *92*, 4231–4237.
- [43] A. Czernichowski, H. Nassar, A. Ranaivosoaarimananana, *Acta Phys. Pol. A* **1996**, *89*, 595–596.
- [44] O. Mutaf-Yardimci, A. V. Saveliev, A. A. Fridman, L. A. Kennedy, *J. Appl. Phys.* **2000**, *87*, 1632–1641.
- [45] T. Kozák, A. Bogaerts, *Plasma Sources Sci. Technol.* **2014**, *23*, 045004.
- [46] T. Kozák, A. Bogaerts, *Plasma Sources Sci. Technol.* **2015**, *24*, 015024.
- [47] R. Aerts, W. Somers, A. Bogaerts, *ChemSusChem* **2015**, *8*, 702–716.
- [48] R. Snoeckx, R. Aerts, X. Tu, A. Bogaerts, *J. Phys. Chem. C* **2013**, *117*, 4957–4970.
- [49] S. Heijckers, R. Snoeckx, T. Kozák, T. Silva, T. Godfroid, N. Britun, R. Snyders, A. Bogaerts, *J. Phys. Chem. C* **2015**, *119*, 12815–12828.
- [50] R. Snoeckx, S. Heijckers, K. Van Wesenbeeck, S. Lenaerts, A. Bogaerts, *Energy Environ. Sci.* **2016**, *9*, 999–1011.
- [51] W. Z. Wang, A. Bogaerts, *Plasma Sources Sci. Technol.* **2016**, *25*, 055025.
- [52] F. Richard, J. M. Cormier, S. Pellerin, J. Chapelle, *J. Appl. Phys.* **1996**, *79*, 2245–2250.
- [53] S. Pellerin, F. Richard, J. Chapelle, J. M. Cormier, K. Musiol, *J. Phys. D* **2000**, *33*, 2407–2419.
- [54] St. Kolev, A. Bogaerts, *Plasma Sources Sci. Technol.* **2015**, *24*, 015025.
- [55] St. Kolev, A. Bogaerts, *Plasma Sources Sci. Technol.* **2015**, *24*, 065023.
- [56] G. Trenchev, St. Kolev, A. Bogaerts, *Plasma Sources Sci. Technol.* **2016**, *25*, 035014.



- [57] S. R. Sun, St. Kolev, H. X. Wang, A. Bogaerts, *Plasma Sources Sci. Technol.* **2016**, *26*, 015003.
- [58] S. R. Sun, H. X. Wang, D. H. Mei, X. Tu, A. Bogaerts, *J. CO<sub>2</sub> Util.* **2017**, *17*, 220–234.
- [59] W. Z. Wang, A. Berthelot, St. Kolev, X. Tu, A. Bogaerts, *Plasma Sources Sci. Technol.* **2016**, *25*, 065012.
- [60] V. Guerra, J. Loureiro, *J. Phys. D* **1995**, *28*, 1903–1918.
- [61] M. Capitelli, C. M. Ferreira, B. F. Gordiets, A. I. Osipov, *Plasma kinetics in atmospheric gases*, Springer Berlin **2000**.
- [62] B. F. Gordiets, C. M. Ferreira, V. L. Guerra, J. M. A. H. Loureiro, J. Nahorny, D. Pagnon, M. Touzeau, M. Vialle, *IEEE Trans. Plasma Sci.* **1995**, *23*, 750–768.
- [63] V. Guerra, P. A. Sá, J. Loureiro, *Eur. Phys. J. Appl. Phys.* **2004**, *28*, 125–152.
- [64] I. A. Kossyi, A. Yu Kostinsky, A. A. Matveyev, V. P. Silkov, *Plasma Sources Sci. Technol.* **1992**, *1*, 207–220.
- [65] A. B. Murphy, *J. Phys. D* **2001**, *34*, R151–R173.
- [66] W. Z. Wang, M. Z. Rong, Y. Wu, J. D. Yan, *J. Phys. D* **2014**, *47*, 255201.
- [67] M. Appl in *Ullmann's Encyclopedia of Industrial Chemistry* Wiley, VCH, Weinheim, **2012**, pp. 139–225.
- [68] E. D. McCollum, F. Daniels, *Ind. Eng. Chem.* **1923**, *15*, 1173–1175.
- [69] W. S. Partridge, R. B. Parlin, B. J. Zwolinski, *Ind. Eng. Chem.* **1954**, *46*, 1468–1471.
- [70] M. Rahman, V. Cooray, *Opt. Laser Technol.* **2003**, *35*, 543–546.
- [71] W. L. Chameides, D. H. Stedman, R. R. Dickerson, D. W. Rusch, R. J. Cicerone, *J. Atmos. Sci.* **1977**, *34*, 143–149.
- [72] N. Rehbein, V. Cooray, *J. Electrostat.* **2001**, *51–52*, 333–339.
- [73] B. S. Patil, N. Cherkasov, J. Lang, A. O. Ibhaddonb, V. Hessel, Q. Wang, *Appl. Catal. B* **2016**, *194*, 123–133.
- [74] C. E. Treanor, *J. Chem. Phys.* **1968**, *48*, 1798–1807.
- [75] T. L. Zhao, Y. Xu, Y. H. Song, X. S. Li, J. L. Liu, J. B. Liu, A. M. Zhu, *J. Phys. D* **2013**, *46*, 345201.
- [76] J. Zhu, J. Gao, A. Ehn, Z. Li, M. Aldén, M. Salewski, Y. Kusano, *Translational, rotational and vibrational temperatures of a gliding arc discharge at atmospheric pressure air* (Eds.: R. Brandenburg, L. Stollenwerk), *14th International Symposium on High Pressure Low Temperature Plasma Chemistry: Book of Contributions*, **2014**, INP Greifswald.
- [77] T. M. Grigorjeva, A. A. Levitsky, S. O. Macheret, L. S. Polak, V. D. Rusanov, A. Fridman, *High Energy Chem.* **1984**, *18*, 268–272.
- [78] B. Benstaali, D. Moussa, A. Addou, J.-L. Brisset, *Eur. Phys. J. Appl. Phys.* **1998**, *4*, 171–179.
- [79] J. H. Yan, C. M. Du, X. D. Li, B. G. Cheron, M. J. Ni, K. F. Cen, *Plasma Chem. Plasma Process.* **2006**, *26*, 31–41.
- [80] B. S. Patil, F. J. J. Peeters, J. A. Medrano, G. van Rooij, F. Gallucci, J. Lang, Q. Wang, V. Hessel, *Plasma nitrogen oxide production from air at atmospheric pressure using a pulse powered milli-scale gliding arc reactor*, **2016**, AIChEJ, revision submitted.
- [81] W. Castle, *Int. J. Refrig.* **2002**, *25*, 158–172.
- [82] S. Pancheshnyi, B. Eismann, G. Hagelaar, L. Pitchford, Computer code zdpplaskin (University of Toulouse, LAPLACE, CNRS-UPS-INP, France) [www.zdpplaskin.laplace.univ-tlse.fr](http://www.zdpplaskin.laplace.univ-tlse.fr), **2008**.
- [83] G. J. M. Hagelaar, L. C. Pitchford, *Plasma Sources Sci. Technol.* **2005**, *14*, 722–733.
- [84] W. Tsang, J. T. Herron, *J. Phys. Chem. Ref. Data* **1991**, *20*, 609–663.
- [85] M. A. A. Clyne, I. S. McDermid, *J. Chem. Soc. Faraday Trans. 1* **1975**, *71*, 2189–2202.
- [86] D. L. Baulch, C. J. Cobos, R. A. Cox, P. Frank, G. Hayman, Th. Just, J. A. Kerr, T. Murrells, M. J. Pilling, J. Troe, R. W. Walker, J. Warnatz, *J. Phys. Chem. Ref. Data* **1994**, *23*, 847–1033.

Manuscript received: January 18, 2017

Revised: February 16, 2017

Accepted Article published: March 8, 2017

Final Article published: April 4, 2017